2024 IEEE/ASME International Conference on Advanced Intelligent Mechatronics (AIM)
July 15-19, 2024. Boston, MA, USA

Brain Computer Interface (BCI)-Enhanced Knee Exoskeleton Control for Assisted Sit-to-Stand Movement

Chunchu Zhu, Sushant Maurya, Jingang Yi, and Ashish Dutta

Abstract— **As the aging and disabled populations grow, the demand for effective assistance in daily activities such as sit-to-stand (STS) has been increasing. Wearable exoskeletons are a promising technology for reducing the effort required for STS. This study explores the sensor fusion of electroencephalography (EEG) signals, which reveal pre-movement intentions, with inertial measurement unit (IMU) data, offering real-time motion information for enhanced knee exoskeleton control in STS assistance. The EEG-IMU sensor fusion approach improves the temporal accuracy and robustness of STS intention detection. By detecting STS intentions with lower latencies, the knee exoskeleton provides timely and smooth support, enhancing the user experience. The proposed method reduces system latency, enabling rapid user-exoskeleton interaction. Experimental results demonstrate the effectiveness of the brain-computer interface (BCI)-enhanced knee exoskeleton for improving STS efficiency and user experience.**

I. Introduction

With increased aging populations, effective assistance, and care services are frequently needed for elders for their daily activities such as sit-to-stand (STS) movements [1]. Wearable exoskeletons and sensors show promise in reducing efforts during personal daily activities (e.g., [2] for STS). Understanding the biomechanics, motor control characteristics, and detecting the human motion intentions is crucial for developing appropriate wearable devices and assistance [3]. Most intention detection methods use wearable sensors such as inertial measurement units (IMUs), electromyography (EMG), or other physical or electrophysiological sensors. One approach involves the analysis of multi-channel myoelectric signals, providing insights into muscle activation sequence and levels during STS movements [4]. Wearable IMUs have been utilized to detect human activities and postural transitions, providing new ways to monitor mobility and fall risk [5]–[8]. Additionally, wearable pendants and shoe devices have been employed to accurately detect STS and gait, potentially assessing fall risk in the elders [9], [10].

While these intention detection methods provide valuable insights for assistive devices, IMU and EMG cannot predict intentions before the actual motion happens. Recent electroencephalography (EEG)-based research suggests that movement intentions can be decoded from scalp recordings before execution, offering insights into motor planning and preparation [11]. However, EEG-only prediction accuracy is insufficient for practical use. Combining EEG and EMG captures both preparatory brain signals and muscle activity related to the movement execution, enabling a comprehensive understanding of user intentions [12]. Accurate movement predictions have been realized and reported by using the EEG and EMG sensor fusion [13], [14].

Despite promising results from EEG-EMG fusion in improving intention detection accuracy, real-time integration and synchronization for accurate gait and motion intention detection remain challenging. Alternatively, IMU measurements provide direct real-time motion data, and wearable IMUs are small-size, inexpensive, and convenient for daily use. IMU data complements EEG signals that indicate user intentions before movement execution. EEG-IMU fusion has been used to develop accurate and power-efficient drowsiness detection systems for activities like driving, mining, and industrial tasks [15]. It has also been applied to detect activities in healthy subjects and those with Parkinson's disease [16], [17]. However, most EEG-IMU integration studies were not developed for real-time applications.

This work explores the feasibility of EEG-IMU sensor fusion for real-time knee exoskeleton control in STS assistance. A machine learning-based fusion scheme is proposed to integrate EEG and IMU measurements, emphasizing efficient, high-accuracy, and low-latency interpretation during STS motion. An impedance exoskeleton controller is integrated with the intention detection system for real-time assistance, providing timely and smooth support for an intuitive and comfortable user experience. We demonstrate the EEG-IMU integration and exoskeleton control design through multiple subject experiments. The main contributions are twofold. First, EEG-IMU fusion reduces system latency in intention detection, allowing rapid exoskeleton response to user commands, and enhancing real-time interaction and seamless assistance. Second, integrating EEG-IMU sensor fusion into exoskeleton systems significantly improves user experience. The significance lies in the complementary nature of EEG and IMU, where EEG provides neural insights on intention and IMU offers real-time kinematic data, enabling more accurate and responsive exoskeleton control.

The rest of the paper is organized as follows. Section II discusses the BCI-based real-time intention detection and the exoskeleton control strategy. Section III introduces the experiment setups. Experimental results and discussion are presented in Section IV and finally, we summarize the concluding remarks in Section V.

This work was supported in part by the US NSF under awards CNS-1932370 and ECCS-2222880.

C. Zhu and J. Yi are with the Department of Mechanical and Aerospace Engineering, Rutgers University, Piscataway, NJ 08854 USA (email: chunchu.zhu@rutgers.edu, jgyi@rutgers.edu).

S. Maurya and A. Dutta are with the Department of Mechanical Engineering, Indian Institute of Technology, Kanpur 208016, India (email: smaurya@iitk.ac.in, adutta@iitk.ac.in).

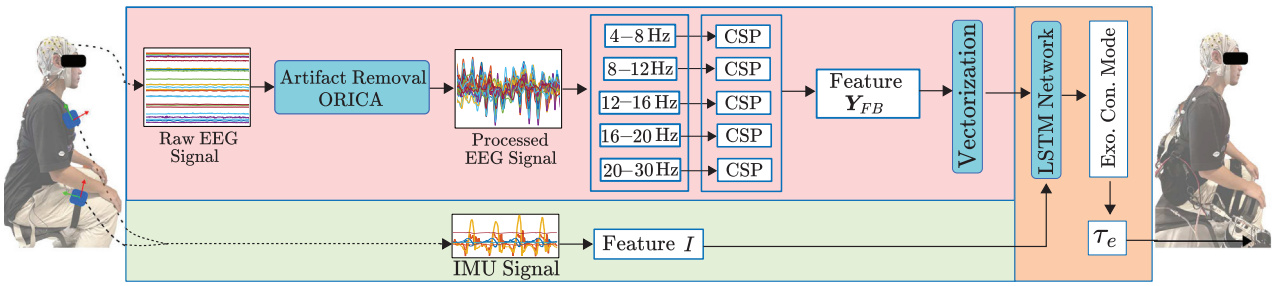

Fig. 1. Overall design of the BCI-enhanced knee exoskeleton control for STS movement.

II. The BCI-Enhanced Exoskeleton Control

In this section, we present the BCI-based human-exoskeleton interface for STS assistance. Fig. 1 illustrates the overall architecture of the system design. In the following, we present the details about the EEG data processing, the EEG-IMU fusion design, and the exoskeleton control.

A. EEG Data Processing

EEG signals are often contaminated with unwanted artifacts, such as those caused by muscle activity, which can hinder accurate interpretation and analysis. Various methods have been proposed to remove muscle-related artifacts from EEG signals [18]. In the context of STS movement, the EEG artifacts are mainly induced by muscle activation. Therefore, the online recursive independent component analysis (ORICA) algorithm was applied to the raw EEG data [19].

To address the issue of dependent source signals caused by the mixing process, we first employ a whitening process to enhance the independence of sources and reduce signal correlations. This involves pre-multiplying the whitening matrix $\boldsymbol{M}$ to the recorded EEG signals $\boldsymbol{X} \in \mathbb{R}^{n\times N}$, where n represents the number of EEG channels, and N denotes the number of samples in the sliding time window under consideration, resulting in whitened signals, denoted as $\boldsymbol{v} = \boldsymbol{M}\boldsymbol{X}$. The whitening matrix $\boldsymbol{M}$ is updated iteratively using the online recursive-least-squares (RLS) whitening formula, known for its fast convergence. The ORICA algorithm aims to find the de-mixing matrix, $\boldsymbol{W}$, to recover the original EEG sources from the whitened signals $\boldsymbol{v}$, that is, $\hat{\boldsymbol{X}} = \boldsymbol{W}\boldsymbol{v}$ is the recovered EEG data [20]. The iterative update of $\boldsymbol{W}$ is obtained by the ORICA algorithm.

The recovered EEG data is transformed into filtered EEG data using the filter bank common spatial pattern (FBCSP) to extract features. FBCSP enhances the performance of the common spatial pattern (CSP) algorithm in motor imagery-based BCIs by autonomously selecting EEG characteristics in different frequency bands [21]. Let $\hat{\boldsymbol{X}} \in \mathbb{R}^{n\times N}$ be the recovered multichannel EEG data matrix. We divide the EEG data into m frequency sub-bands using bandpass filters. Let $\hat{\boldsymbol{X}}_j$ be the EEG data in the jth frequency sub-band. For each $\hat{\boldsymbol{X}}_j$, we apply CSP to extract spatial filters $\boldsymbol{U}_j$ that maximize the variance differences and discriminate between two classes of EEG signals (e.g., sit vs. stand motor imagery). The filtered EEG data $\boldsymbol{Y}_j$ is obtained by projecting $\hat{\boldsymbol{X}}_j$ onto the spatial filters $\boldsymbol{U}_j$, that is, $\boldsymbol{Y}_j = \boldsymbol{U}_j^T\hat{\boldsymbol{X}}_j$. The final FBCSP features are obtained by concatenating the CSP features $\boldsymbol{Y}_i$ from all frequency bands as $\boldsymbol{Y}_{\text{FB}} = [\boldsymbol{Y}_1, \boldsymbol{Y}_2, \ldots, \boldsymbol{Y}_m]$, representing the autonomous selection of key temporal-spatial discriminative EEG characteristics for motor imagery classification.

B. EEG-IMU Sensor Fusion

To detect human intention, we propose a sensor fusion approach that combines the EEG features and IMU data. The FBCSP features $\boldsymbol{Y}_{\text{FB}}(t)$ and the IMU data $\boldsymbol{I}(t)$ are vectorized as input for a classifier to distinguish between the different motor imagery tasks. In the STS context, the intention to transit from a seated to a standing position inherently involves temporal patterns and sequences, both in terms of cognitive decision-making and physical motion dynamics. The long short-term memory (LSTM) network is a type of recurrent neural network (RNN) architecture specifically designed to capture long-term dependencies in time series data. LSTMs demonstrate exceptional proficiency in deciphering intricate temporal nuances. This capability enables them to recognize subtle intention or motion cues that may span across varying time scales and understand the relationship between these data. Therefore, we use the LSTM network to capture both the temporal and spatial dependencies to improve the accuracy and lower the detection latency of the system.

Fig. 2 shows the detailed configuration of the LSTM network. It is composed of LSTM cells, which contain memory cells, input gates, forget gates, and output gates. The outputs of the LSTM pass through a Dropout layer before they go through a fully connected layer with the rectified linear unit (ReLU) to prevent model overfitting. The hidden layer is connected to the Softmax activation function, where the class scores are converted to probabilities for different activities. Similar LSTM-based gait activity and pose estimation schemes were developed for human or animal locomotion for real-time applications [7], [22].

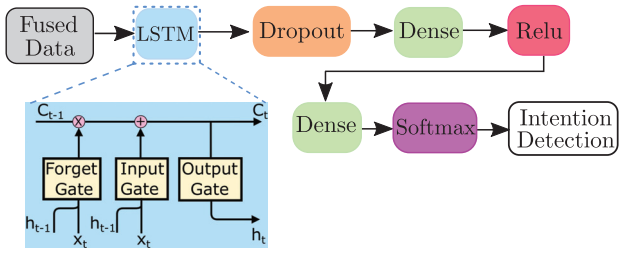

Fig. 2. Schematic of the LSTM-based intention recognition.

C. Exoskeleton Control

Fig. 3(a) illustrates the overall exoskeleton control flowchart. The exoskeleton controller is built on the BCI-enhanced intention detection system. Once the STS intention is detected through the system, the knee exoskeleton control is activated and assistive knee torque is then applied.

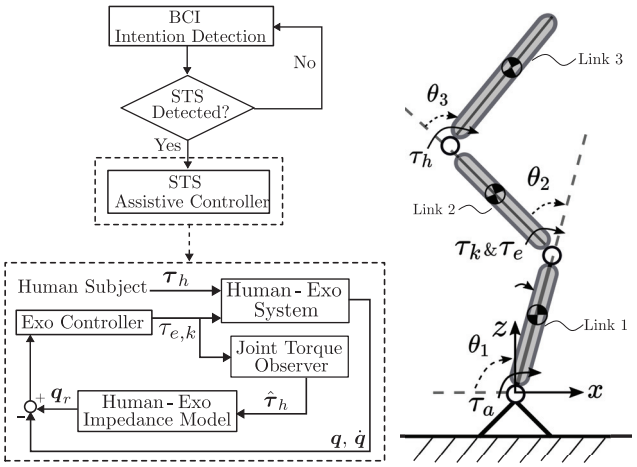

Fig. 3. (a) The flowchart schematic of the BCI-enhanced exoskeleton control design. (b) The schematic of the 3-DOF planar robotic system to represent the human STS movement.

The knee joint plays a crucial role in STS motion, and an effective controller ensures smooth transitions between phases. Assuming the human knee joint and exoskeleton are aligned and the movements are synchronous, the human-exoskeleton system can be modeled as a 3 degree-of-freedom (DOF) system in the sagittal plane. Fig. 3(b) illustrates the schematic of the modeling configuration. The human-exoskeleton system is captured by three links: shank or exoskeleton lower link (link 1), thigh or exoskeleton upper link (link 2), and upper body (link 3). Denoting the ankle, knee, and hip angles as θ_1, θ_2, and θ_3, respectively, we introduce $\boldsymbol{q} = [\theta_1 \ \theta_2 \ \theta_3]^T$ as the generalized coordinate. Similar to the work in [23], the STS motion dynamics are described as

$$\boldsymbol{D}(\boldsymbol{q})\ddot{\boldsymbol{q}} + \boldsymbol{C}(\boldsymbol{q}, \dot{\boldsymbol{q}})\dot{\boldsymbol{q}} + \boldsymbol{G}(\boldsymbol{q}) = \boldsymbol{\tau}_h + \boldsymbol{\tau}_e, \tag{1}$$

where $\boldsymbol{D}(\boldsymbol{q}), \boldsymbol{C}(\boldsymbol{q}, \dot{\boldsymbol{q}})$, and $\boldsymbol{G}(\boldsymbol{q})$ are the inertia, Coriolis, and gravity matrices, respectively. The torque inputs $\boldsymbol{\tau}_h = [\tau_a \ \tau_k \ \tau_h]^T$ are human joint torques at ankle, knee, and hip joints, and $\boldsymbol{\tau}_e = [0 \ \tau_{e,k} \ 0]^T$ is the applied exoskeleton torque at the knee joint. Similar to [2], an observer is applied to estimate the driving joint torques $\hat{\boldsymbol{\tau}}_h$. With the estimated $\hat{\boldsymbol{\tau}}_h$, an impedance compensation model is proposed as the following inverse dynamics to estimate and obtain the desired motion profile $\boldsymbol{q}_r$.

$$\boldsymbol{\lambda}\left[\boldsymbol{D}(\boldsymbol{q})\ddot{\boldsymbol{q}}_r + \boldsymbol{C}(\boldsymbol{q}, \dot{\boldsymbol{q}})\dot{\boldsymbol{q}}_r + \boldsymbol{G}(\boldsymbol{q})\right] = \hat{\boldsymbol{\tau}}_h, \tag{2}$$

where $\ddot{\boldsymbol{q}}_r$ and $\dot{\boldsymbol{q}}_r$ are the estimated joint acceleration and velocity references, respectively. $\boldsymbol{\lambda} = \mathrm{diag}(1, \lambda_k, 1)$ and $\lambda_k \in (0, 1]$ is the assistive ratio, designed as $\lambda_k = \eta_1 \tanh((\theta_2 - \theta_{st}/2)/\eta_2) + \eta_3$, with adjustable parameters η_1, η_2, and η_3 and θ_{st} is the knee angle at natural stance.

The overall controller design logic is also illustrated in Fig. 3(a). With the computed joint angle profile $\boldsymbol{q}_r$ by inverse dynamics (2), the exoskeleton control torque is design as

$$\tau_{e,k} = k_p(\theta_2 - \theta_r) + k_d(\dot{\theta}_2 - \dot{\theta}_r), \tag{3}$$

where k_p and k_d are the control gains.

III. Experiments

In this section, a synchronized EEG and IMU signal acquisition experiment is designed to verify the effectiveness of the proposed BCI-enhanced knee exoskeleton control.

A. Data Collection and Processing

Fig. 4(a) shows the wearable sensing and exoskeleton systems and their interconnections. Two IMUs (LP-RESEARCH Inc.) were attached to the subject's right thigh and trunk to collect 3-axial orientation angles, gyroscope rates, and linear accelerations. A motion capture system (10 Vicon Vantage cameras) was used to obtain ground-truth trunk positions for validation. A 32-channel wireless high-density EEG system with active electrodes (Brain Products GmbH) was connected to the Liveamp wireless adapter, and EEG data was streamed through Lab Streaming Layer (LSL) software. Peripheral EEG channels susceptible to eye blinks and facial/cranial muscle activity were removed from analysis, the retained 23 EEG channels include the frontal cortex (F7, F3, Fz, F4, and F8), the central cortex (FC5, FC1, FC2, FC6, C3, Cz, and C4), the parietal cortex (CP1, CP2, P3, Pz, and P4), left temporal (T7, CP5, P7), and right temporal (T8, CP6, P8). Data from all sensors was synchronized and collected at 100 Hz through a portable embedded computer (Intel NUC7i7DNK, Intel Corp.).

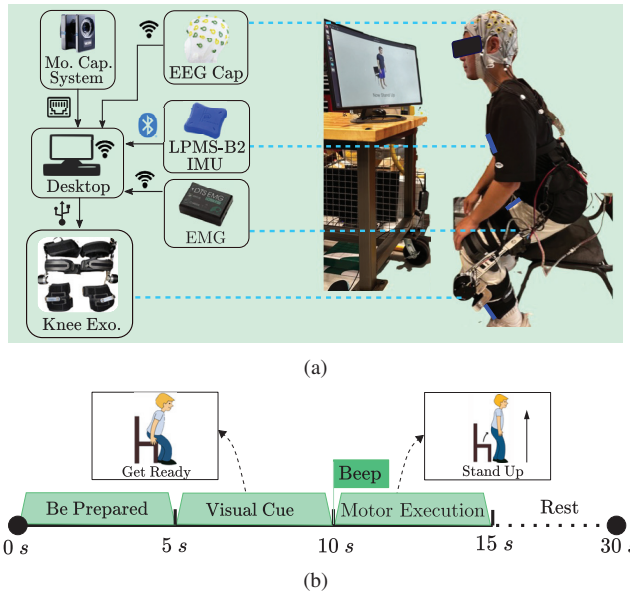

Fig. 4. (a) Schematic of the wearable sensing system, the interconnections, and the experiment setup. (b) The synchronous acquisition diagram that illustrates the experiment protocols during the STS movement.

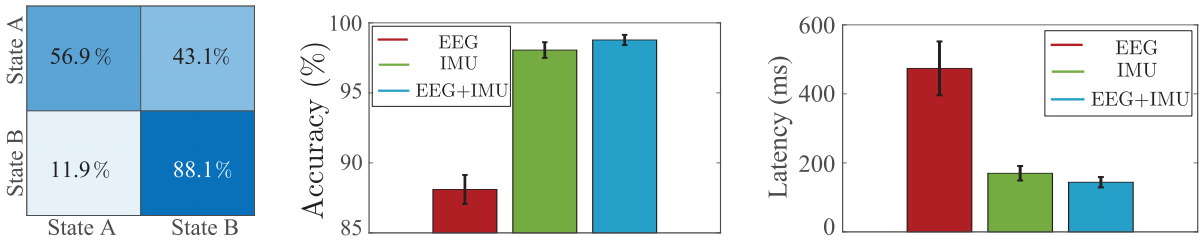

(a) (b) (c)

Fig. 5. (a) Confusion matrix for detecting States A and B using EEG features in offline STS classification. The x-axis is the predicted labels and the y-axis is the true label. (b) Offline prediction accuracy and (c) Detection latency comparison for three sensing data sets.

Fig. 4(a) also shows the quasi-direct drive bilateral knee exoskeleton with high-torque, high-backdrivability, and high-bandwidth features [24], [25]. The low-level controller received states from the high-level controller (Linux embedded system) and conducted torque feedback control for the exoskeleton. The parameter values of the used controller were: $k_p = 15$, $k_d = 0.08$, $\lambda_k = 0.2$, $\eta_1 = 0.2$, $\eta_2 = -4$, and $\eta_3 = 0.8$. The raw EEG and IMU data were recorded, followed by the pre-processing using a 1 s sliding window with a 0.2 s shift. The EEG data was then processed to extract the features of the neural network. Similar to [26], $m = 6$ EEG frequency sub-bands were selected in this work, i.e., 4-8, 8-12, 12-16, 16-20, and 20-30 Hz.

In the experiments, 5 wireless surface EMGs (DTS EMG, Noraxon, Inc., AZ, USA) were attached to the right leg knee extensor muscles [rectus femoris (RFEM), vastus lateralis (VLAT), and vastus medialis (VMED)] and knee flexor muscles [biceps femoris (BFLH) and semitendinosus (SEMT)] to measure muscle activations and effort during STS tasks with and without assistive torques. The EMG data were collected at 1500 Hz, bandpass filtered (10-500 Hz), normalized to the average muscle activation throughout the trial, rectified, and analyzed using the root mean square average.

B. Experimental Protocols

Five young subjects, naive BCI users (Five males; age: 25.6±2.4 years; height: 175.8±7 cm; weight: 67.4±12.9 kg) participated in the experiments. The subjects were self-reported as healthy without any known neurophysiological or musculoskeletal disorders. An informed consent form was signed by all the subjects, and the Institutional Review Board (IRB) at Rutgers University approved the testing protocols.

Fig. 4(b) illustrates the human subject experimental sequence during the STS movement. The experiments consisted of offline training and real-time validation sessions. During offline data collection, subjects naturally seated in front of the computer, and followed the synchronous experimental paradigm to perform the corresponding actions (first performed motor imagination and then the corresponding STS actions). The protocol details are as follows:

- 0-5 s: The screen reminded the subject to be prepared for the instructions.
- 5-10 s: A picture about STS movement was played on the screen, reminding the subjects of the movement to perform motor imagery (State A).
- 10-15 s: At 10 s, the computer emitted a beep prompt and a '↑' pattern appeared on the screen, prompting the subject to perform the STS task execution corresponding to the motor imagery (State B).
- 15-30 s: At 15 s, the computer emitted a beep prompt for the second time and showed "Relax and Sit Down" on the screen, reminding the subject that the ongoing trial was over and indicating the start of the next 15 s of resting interval.

The offline training session contained 40 trials for each subject. A 5-min break was given after 10 trials.

In the real-time validation session, subjects were equipped with the exoskeleton and followed the same paradigm. An additional IMU sensor on the right shank captured the knee joint angle. The exoskeleton provided assistive torques based on detected intentions, and each subject completed 10 real-time trials. To compare results across subjects, the STS gait percentage was normalized based on knee joint angle progression. Given the knee angle $\theta_2(t)$, the gait percentage s is computed as:

$$s = \frac{\int_{t_0}^{t} \theta_2(t)dt}{\int_{t_0}^{t_f} \theta_2(t)dt} \times 100\%,$$

where t_0 and t_f represent the starting time (seated) and the finishing time (standing) throughout the STS motion.

IV. Results

A. Experimental Results

Offline experimental results validate the LSTM network's ability to distinguish States A and B using EEG FBCSP features alone. Fig. 5(a) shows the model struggled to classify the states, especially during motor imagery, confirming intention detection before movement but distinguishing motor imagery from execution requires spatial data (e.g., IMU). Comparing offline STS state classification using three sensing data sets for all subjects, see Fig. 5(b), the detection accuracy is 88.1 ± 1 % for EEG FBCSP features only, 98.1±0.6 % with IMU data only, and 98.8±0.4 % for EEG-IMU feature fusion. Table I provides detailed comparisons among five subjects, with the best sensor fusion performance exceeding 99 %. Fig. 5(c) shows that average detection latencies are 474±78 ms, 170±21 ms, 144±15 ms for EEG only, IMU only, and EEG-IMU sensor fusion, respectively.

Real-time BCI-enhanced exoskeleton control was evaluated based on the algorithm's detection feasibility and the

TABLE I

OFFLINE COMPARISON OF THE STS PREDICTION ACCURACY

Group	S1	S2	S3	S4	S5	Ave. Acc.
EEG only (%)	87.3	88.6	86.9	88.2	89.5	88.1
IMU only (%)	97.5	98.2	98.9	97.6	98.1	98.1
EEG-IMU (%)	98.5	99.1	99.1	98.3	98.9	98.8

TABLE II

REAL-TIME COMPARISON OF THE ACCURACY, TPR, AND LATENCY

Group	S1	S2	S3	S4	S5	Ave.
Acc (%)	96.2	90.6	89.9	93.2	90.5	92.1
TPR (%)	97.5	93.4	96.9	94.6	95.2	95.5
Latency (ms)	142	158	147	143	151	148

effectiveness of impedance control in reducing muscle effort. To this end, we focus on the performance in State B (actual STS motion). The detection accuracy is defined as:

$$Acc = \frac{n_{\text{correct}}}{n_{\text{total}}} \times 100\%,$$

where n_{total} is the total number of samples, and n_{correct} is the number of samples that were classified correctly with the model. The sensor fusion performance of the system was also evaluated using the true positive rate (TPR), which indicates the percentage of times that STS movement was detected correctly,

$$TPR = \frac{TP}{TP + FN} \times 100\%,$$

where TP is the true positives and FN is the false negatives. Table II lists the accuracy, TPR, and average latency for each subject. Real-time STS experiments achieved an average accuracy of 92 % and TPR of 95 %. With the EEG-IMU sensor fusion, the STS movements are detected around 150 ms on average after the motion happens.

Fig. 6(a) shows the exoskeleton output torque $\tau_{e,k}$ from all subjects. Notably, the exoskeleton torques exhibit greater variance during the initial STS phase, stabilizing in the latter phase. This variance is attributed to additional exertion at gait initiation and variations in subjects' standing velocities. EMG amplitudes varied among individuals due to movement and musculoskeletal differences, so we focused on comparing muscle activation reduction percentages. Fig. 6(b) shows the EMG data for a representative subject during five STS repetitions. Knee extensor muscle (RFEM, VLAT, VMED) activation was significantly reduced with assistive torques, especially in the early STS phase, indicating the exoskeleton's role in assisting human motion. Table III summarizes the muscle activation reductions among the subjects. Average peak muscle activities of RFEM, VLAT, VMED, and BFLH were reduced by 13.2%, 3.8%, 9.7%, and 9.1%, respectively, compared to no exoskeleton condition. Although SEMT activation decreased initially, it increased towards the end, possibly due to individual compensatory mechanisms or the exoskeleton's impact on muscle workload distribution. Further analysis is needed to ensure harmonious assistance and reduce non-typical muscle activation.

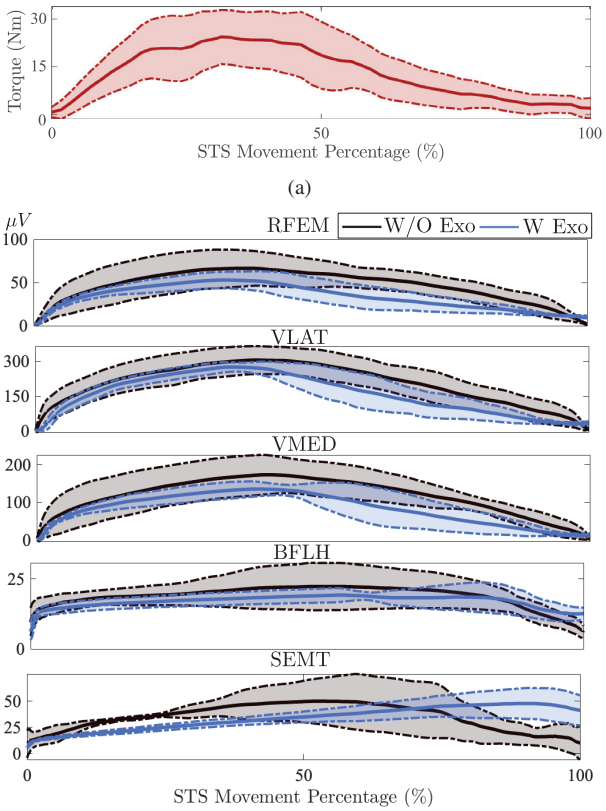

Fig. 6. (a) Knee exoskeleton torque outputs during STS movements. (b) EMG patterns for one subject during five STS movements with and without the exoskeleton controller. The solid lines are the mean values and the shaded areas are the standard deviations.

TABLE III

MUSCLE ACTIVATION REDUCTION PERCENTAGE ACROSS ALL SUBJECTS

Muscles	S1	S2	S3	S4	S5	Ave.
RFEM (%)	−19.7	−14.9	−13.9	−7.4	−10.2	−13.2
VLAT (%)	−9.3	−1.2	−3.1	−0.7	−5.1	−3.8
VMED (%)	−20.1	−7.1	−7.9	−3.5	−10.1	−9.7
BFLH (%)	−16.8	−8.2	−6.1	−4.2	−10.4	−9.1
SEMT (%)	−1.5	4.1	−0.4	4.5	3.9	2.2

B. Discussion

The proposed sensor fusion algorithm integrates EEG and IMU features for accurate and robust human intention detection, providing a comprehensive view of user intentions. The LSTM network effectively captures the dynamic nature of human intentions by modeling temporal dependencies in the fused sensor data. Our findings demonstrate that STS movement intentions can be detected solely from EEG features, even before motion initiation, which has significant implications for knee exoskeleton control.

The EEG-IMU sensor fusion technique can be applied in various exoskeleton scenarios, such as rehabilitation, daily-life assistance, and construction worksites. As highlighted in [27], exoskeletons must exhibit reaction times surpassing physiological limits to enhance user balance during various postures and movements. Reducing response times is crucial, as latency profoundly impacts user experience,

satisfaction, sense of control, and interaction with the exoskeleton. Fig. 5(c) shows average detection latency times of 170 ± 21 ms and 144 ± 15 ms for IMU only and EEG-IMU sensor fusion, respectively. The significance of latency reduction, even by 30-50 ms, cannot be understated in the exoskeleton domain, leading to tangible usability enhancements and improved user outcomes, particularly in rehabilitation contexts where precise movements are vital for effective therapies.

Although our study has made progress in real-time decoding of motor imagery for STS movements, some limitations remain, such as the lack of an explicit comparison of muscle activation under EEG-IMU fusion against IMU only or assist-as-needed controllers in Table III. Future work will conduct comprehensive comparisons, develop new metrics to objectively capture graceful human-exoskeleton interactions, uncover the relationship between EEG and kinematic data during motion, increase participant sample size, use more EEG active electrodes, quantify human-exoskeleton interaction comfort, and refine signal processing techniques.

V. Conclusion

This study introduces a machine learning-based approach that fuses EEG and IMU data for human STS intention detection. The approach combines FBCSP features from EEG data with IMU velocity and acceleration features, capturing spatial and temporal characteristics of both brain and body. A synchronized EEG and IMU data acquisition experiment was designed to verify the effectiveness of the proposed model. Results showed promising performance in detecting movement onset and emphasized the potential of our human-exoskeleton interface in reducing muscle activation through the proposed impedance controller. This work contributes to the growing field of EEG-based intention detection and its applications in exoskeleton technology.

References

[1] H. Wang, S. Xu, J. Fu, X. Xu, Z. Wang, and R. S. Na, "Sit-to-stand (sts) movement analysis of the center of gravity for human–robot interaction," *Front. Neurorobot.*, vol. 16, p. 863722, 2022.

[2] W. Huo, H. Moon, M. A. Alouane, V. Bonnet, J. Huang, Y. Amirat, R. Vaidyanathan, and S. Mohammed, "Impedance modulation control of a lower-limb exoskeleton to assist sit-to-stand movements," *IEEE Trans. Robotics*, vol. 38, no. 2, pp. 1230–1249, 2021.

[3] A. Tsukahara, R. Kawanishi, Y. Hasegawa, and Y. Sankai, "Sit-to-stand and stand-to-sit transfer support for complete paraplegic patients with robot suit hal," *Adv. Robot.*, vol. 24, no. 11, pp. 1615–1638, 2010.

[4] S. Bhardwaj, A. A. Khan, and M. Muzammil, "Lower limb rehabilitation using multimodal measurement of sit-to-stand and stand-to-sit task," *Disabil. Rehabil.: Assist. Tech.*, vol. 16, no. 5, pp. 438–445, 2021.

[5] Y. Huang, Y. Liu, R. Yang, X. Zhang, J. Yi, J. P. Ferreira, and T. Liu, "Real-time intended knee joint motion prediction by deep-recurrent neural networks (RNNs)," *IEEE Sensors J.*, vol. 19, no. 23, pp. 11 503–11 509, 2019.

[6] L. Wang, Y. Sun, Q. Li, T. Liu, and J. Yi, "Two shank-mounted IMUs-based gait analysis and classification for neurological disease patients," *IEEE Robot. Automat. Lett.*, vol. 5, no. 2, pp. 1970–1976, 2020.

[7] S. Chen, S. S. Bangaru, T. Yigit, M. Trkov, C. Wang, and J. Yi, "Real-time walking gait estimation for construction workers using a single wearable inertial measurement unit (IMU)," in *Proc. IEEE/ASME Int. Conf. Adv. Intelli. Mechatronics*, Delft, Netherlands, 2021, pp. 753–758.

[8] C. Zhu, F. Han, and J. Yi, "Wearable sensing and knee exoskeleton control for awkward gaits assistance," in *Proc. IEEE Conf. Automat. Sci. Eng.*, Mexico City, Mexico, 2022, pp. 2393–2398.

[9] A. Ejupi, M. Brodie, S. R. Lord, J. Annegarn, S. J. Redmond, and K. Delbaere, "Wavelet-based sit-to-stand detection and assessment of fall risk in older people using a wearable pendant device," *IEEE Trans. Biomed. Eng.*, vol. 64, no. 7, pp. 1602–1607, 2016.

[10] Z. He, J. Yi, and T. Liu, "A wearable sensing and training system: Towards gait rehabilitation for elderly patients with knee osteoarthritis," *IEEE Sensors J.*, vol. 19, no. 14, pp. 5936–5945, 2019.

[11] T. C. Bulea, S. Prasad, A. Kilicarslan, and J. L. Contreras-Vidal, "Sitting and standing intention can be decoded from scalp EEG recorded prior to movement execution," *Front. Comput. Neurosci.*, vol. 8, 2014, article 376.

[12] J. Tryon, E. Friedman, and A. L. Trejos, "Performance evaluation of EEG/EMG fusion methods for motion classification," in *Proc. IEEE Int. Conf. Rehab. Robot.*, Toronto, Canada, 2019, pp. 971–976.

[13] K. Shi, R. Huang, F. Mu, Z. Peng, K. Huang, Y. Qin, X. Yang, and H. Cheng, "A novel multimodal human-exoskeleton interface based on EEG and sEMG activity for rehabilitation training," in *Proc. IEEE Int. Conf. Robot. Autom.*, Philadelphia, PA, 2022, pp. 8076–8082.

[14] S. Tortora, L. Tonin, C. Chisari, S. Micera, E. Menegatti, and F. Artoni, "Hybrid human-machine interface for gait decoding through Bayesian fusion of EEG and EMG classifiers," *Front. Neurorobot.*, vol. 14, 2020, article 582728.

[15] V. J. Kartsch, S. Benatti, P. D. Schiavone, D. Rossi, and L. Benini, "A sensor fusion approach for drowsiness detection in wearable ultra-low-power systems," *Inform. Fusion*, vol. 43, pp. 66–76, 2018.

[16] M. Graña, M. Aguilar-Moreno, J. De Lope Asiain, I. B. Araquistain, and X. Garmendia, "Improved activity recognition combining inertial motion sensors and electroencephalogram signals," *Int. J. Neural Sys.*, vol. 30, no. 10, 2020, artitle 2050053.

[17] M. Abtahi, S. Bahram Borgheai, R. Jafari, N. Constant, R. Diouf, Y. Shahriari, and K. Mankodiya, "Merging fNIRS-EEG brain monitoring and body motion capture to distinguish Parkinsons disease," *IEEE Trans. Neural Syst. Rehab. Eng.*, vol. 28, no. 6, pp. 1246–1253, 2020.

[18] W. Mumtaz, S. Rasheed, and A. Irfan, "Review of challenges associated with the EEG artifact removal methods," *Biomed. Signal Processing and Control*, vol. 68, 2021, article 102741.

[19] S.-H. Hsu, L. Pion-Tonachini, T.-P. Jung, and G. Cauwenberghs, "Tracking non-stationary EEG sources using adaptive online recursive independent component analysis," in *Proc. IEEE Int. Conf. Eng. Med. Bio. Soc.*, Milan, Italy, 2015, pp. 4106–4109.

[20] S.-H. Hsu, T. R. Mullen, T.-P. Jung, and G. Cauwenberghs, "Real-time adaptive EEG source separation using online recursive independent component analysis," *IEEE Trans. Neural Syst. Rehab. Eng.*, vol. 24, no. 3, pp. 309–319, 2016.

[21] N. Padfield, J. Zabalza, H. Zhao, V. Masero, and J. Ren, "Eeg-based brain-computer interfaces using motor-imagery: Techniques and challenges," *Sensors*, vol. 19, no. 6, p. 1423, 2019.

[22] T. Yigit, F. Han, E. Rankins, J. Yi, K. H. McKeever, and K. Malinowski, "Wearable inertial sensor-based limb lameness detection and pose estimation for horses," *IEEE Trans. Automat. Sci. Eng.*, vol. 19, no. 3, pp. 1365–1379, 2022.

[23] S. Chen, D. Stevenson, S. Yu, M. Mioskowska, J. Yi, H. Su, and M. Trkov, "Wearable knee assistive devices for kneeling tasks in construction," *IEEE/ASME Trans. Mechatronics*, vol. 26, no. 4, pp. 1989–1996, 2021.

[24] S. Yu, T.-H. Huang, X. Yang, C. Jiao, J. Yang, H. Hu, S. Zhang, Y. Chen, J. Yi, and H. Su, "Quasi-direct drive actuation for a lightweight hip exoskeleton with high backdrivability and high bandwidth," *IEEE/ASME Trans. Mechatronics*, vol. 25, no. 4, pp. 1794–1802, 2020.

[25] C. Zhu and J. Yi, "Knee exoskeleton-enabled balance control of human walking gait with unexpected foot slip," *IEEE Robot. Automat. Lett.*, 2023, in press.

[26] N. Triana-Guzman, A. D. Orjuela-Cañon, A. L. Jutinico, O. Mendoza-Montoya, and J. M. Antelis, "Decoding EEG rhythms offline and online during motor imagery for standing and sitting based on a brain-computer interface," *Front. Neuroinform.*, vol. 16, p. 961089, 2022.

[27] O. N. Beck, M. K. Shepherd, R. Rastogi, G. Martino, L. H. Ting, and G. S. Sawicki, "Exoskeletons need to react faster than physiological responses to improve standing balance," *Sci. Robot.*, vol. 8, no. 75, p. eadf1080, 2023.